PHYSICAL REVIEW B **83**, 125312 (2011)

Epitaxial lateral overgrowth in the system Si/SiO$_x$/Si: The influence of residual oxygen at the interface

M. Hanke
Paul-Drude Institut für Festkörperelektronik, Hausvogteiplatz 5-7, D-10117 Berlin, Germany

R. Köhler, P. Schäfer, D. Lübbert, I. Häusler, and W. Neumann
Humboldt-Universität zu Berlin, Institut für Physik, Newtonstraße 15, D-12489 Berlin, Germany

P. Modregger
Paul Scherrer Institut, CH-5232 Villigen PSI, Switzerland

T. Boeck
Institut für Kristallzüchtung, Max-Born-Straße 2, D-12489 Berlin, Germany

T. Baumbach
Institut für Synchrotron Strahlung, Forschungszentrum Karlsruhe, D-76344 Eggenstein-Leopoldshafen, Germany
(Received 12 August 2010; revised manuscript received 22 December 2010; published 21 March 2011)

We have studied epitaxial lateral overgrowth from the liquid phase in the system Si/SiO$_x$/Si using a dedicated, synchrotron-based x-ray diffraction setup (topomicroscopy) and transmission electron microscopy. A combination of high angular resolution in reciprocal space with a high spatial resolution in real space may probe lattice tilts in the microradian range on a micrometer scale. We attribute the observed curvature of the silicon lamella to an oxygen loss within the SiO$_x$ layer. Finite-element calculations on the elastic strain distribution and a numerical description of the x-ray scattering process strongly support this scenario.

DOI: 10.1103/PhysRevB.83.125312 PACS number(s): 81.15.Lm, 87.59.−e, 02.70.Dh

I. INTRODUCTION

Epitaxial lateral overgrowth (ELO) is successfully used in order to reduce dislocation densities.[1] More than a decade ago ELO-based superbright GaN light-emitting diodes were impressively demonstrated.[2] However, in many cases a considerable curvature or tilt of the ELO layer is observed.[3] Additionally the crystalline quality of ELO layers strongly depends on the stripe orientation.[4] There are several hypotheses regarding the origin of those effects. For the system Si/SiO$_2$/Si grown by means of liquid-phase epitaxy (LPE) adhesive forces or surface tension of the melt are proposed as origins of the observed curvature.[5,6] It was further argued that the misorientation of GaN stripes observed in the systems GaN/SiO$_2$ and GaN/Al$_2$O$_3$ grown with metal-organic chemical vapor deposition is due to a gradual thinning of the SiO$_2$ mask.[7,8] A subsequently thinner mask can be attributed to etching, densification during growth, or capillary stresses, which are related to the balance between reduced surface energy and dislocation energy. However, clear evidence for one of those hypotheses is still missing. On the other hand, it might have a considerable effect on the technology of ELO, if the atomistic mechanism of these undesirable effects could be elucidated.

Since high dislocation densities might screen the true origin of the effects, it is consequently advantageous to consider a dislocation-free model system, which is in our case Si/SiO$_2$/Si. Within another context this system was already extensively studied by Bauser and co-workers (see, e.g., Bergmann[9]) in dependence on growth conditions and substrate orientation. From a technological point of view SiO$_2$ is interesting as well since it is frequently used for the ELO of GaN.[10]

In Ref. 6 it was shown that the lattice curvature of the overgrowth lamella becomes absent as soon as the underlying oxide layer is removed by etching. Imagining that the epitaxial layer is intentionally curved back as before etching by applying external forces starting at the growth window and proceeding toward the outer edge of the lamella in a zipperlike fashion, it becomes obvious that the strongest forces are at every moment present at the start point and at this imaginary slider. Consequently the clues to the forces present during growth will be found at two positions: close to the growth window edge and the outer layer edge. In order to check this hypothetical model we need a method which compares deformations over the complete layer area with sufficiently good spatial resolution.

It is well known that x-ray diffraction topography is extremely sensitive to deformations and can image large sample areas. However, in its conventional application its spatial resolution is rather limited. Therefore, we have applied a combination (topomicroscopy) of two techniques, namely, rocking curve imaging[11] and Bragg magnification.[12] By means of the latter a spatial resolution in the submicrometer range is achieved. This is basically limited by diffraction effects in the sample to about 1 μm.

II. SAMPLES

With the above-mentioned growth experiments of Bergmann[9] and the related papers,[6,13] there existed a sound basis for experiments aimed at deformation in such samples. There were some samples of Bauser and co-workers available which were compared with our recently grown ones.[14] Investigations by means of atomic force microscopy, scanning electron microscopy, transmission electron microscopy, and x-ray topography showed that these samples were completely comparable; that time had not produced detectable structural changes. Our growth experiments confirmed the above-mentioned earlier results in that the lattice curvature was mainly dependent on the local thickness of the epitaxial layer at growth conditions (see below) optimal in view of perfect overgrowth, lateral width, and crystallographic quality.

The sample considered in the following was grown as follow: The (111)-oriented silicon substrates as used for the growth are miscut by 0.33° in the $[11\bar{2}]$ direction. The seed windows are made of rectangles with lengths of 500 and 2000 μm, respectively, and widths of 20 μm. Therefore, the thermal oxide (thickness about 60 nm) was locally removed by means of photolithography. Indium was used as a solvent for the LPE at growth temperatures between 920 and 880 °C. As already pointed out, the vertical growth of the lamella stops as soon as an upper (111) facet has developed.[13] Subsequently, lateral growth starts if the thickness above the oxide reaches values between 0.5 and 1 μm. The majority of the lateral overgrowth lamella are defect-free. At a few large lamella, dislocations can be observed running in $\langle 110\rangle$ directions; these are not typical dislocations because their main lengths are situated at the interface between the epitaxial layer and the oxide. Since the growth process occurs extremely close to equilibrium the nucleation on $\{111\}$ planes can be effectively suppressed. Therefore the top sides of the lamella are single (111)-type planes which are, however, not plane but curved. This is schematically shown in Fig. 1, which also depicts the crystallographic orientations and the seed window dimensions.

The x-ray topograph in Fig. 2 represents about one-fourth of the complete $20 \times 20\ \mathrm{mm}^2$ sample used for the synchrotron experiments. It was taken by means of x-ray double-crystal topography. These contrasts are mainly due to deformations in the substrate[6] except in a rather narrow region close to the seed window. They are caused by the epitaxial lamella, but these themselves are not directly visible in the topograph because of the strong tilt related to the curvature of the lamella, as will be discussed later.

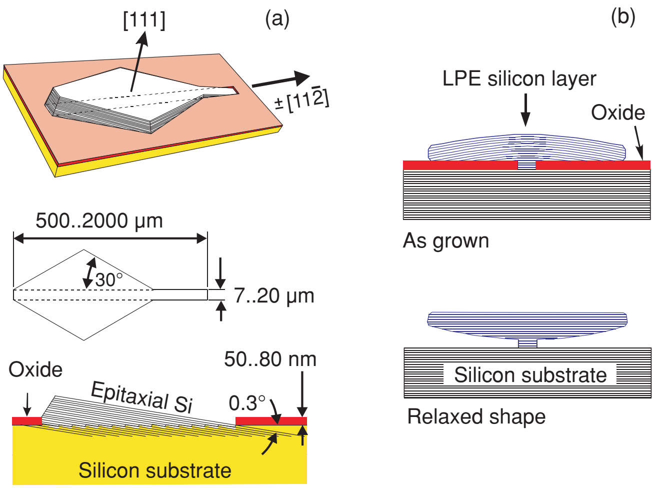

FIG. 1. (Color online) Geometry of the ELO samples: (a) crystallographic directions and dimensions and (b) schematic cross section. The (111) net planes of the epitactic layer are curved after growth. However, they are completely flat after removal of the oxide layer by etching.

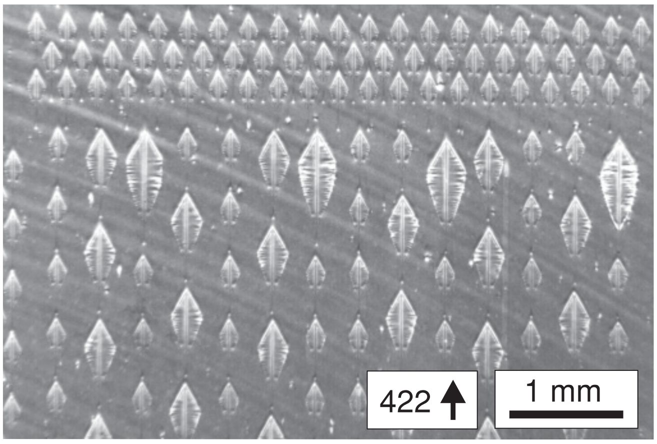

FIG. 2. Laboratory x-ray topograph of the sample used for the present synchrotron experiments. (422) reflection, Cu $K\alpha_1$ radiation, diffraction plane parallel to the seed windows.

III. EXPERIMENT

All samples were investigated by means of optical microscopy, atomic force and scanning electron microscopy, and x-ray double-crystal topography. As indicated before, we have used rocking curve imaging[15]—a method which was successfully applied to the investigation of GaN ELO.[16] From the experimental point of view this is based on taking series of topographs at stepwise changes of diffraction conditions. By changing the incidence angle rocking curves can be extracted at individual local positions, or comparable curves can be obtained depending on other diffraction conditions. These dependencies can be evaluated with consideration of different aspects, e.g., rocking curve shifts and changes of rocking curve widths, etc.

In order to simultaneously study crystal deformation on the micrometer scale in direct space and on the microradian scale in reciprocal space, we developed a dedicated experimental setup: the topomicroscope (TM). The TM may be regarded as a combination of a Bragg magnifier (BM), an x-ray phase-contrast imaging technique with submicrometer spatial resolution, and the aforementioned rocking curve imaging.

Bragg magnification means magnification in two perpendicular directions downstream of the sample by two analyzer crystals providing asymmetric Bragg reflections. Our general setup of the Bragg magnifier was already presented.[17] However, in the topomicroscope (Fig. 3), a complete BM including a charge-coupled device (CCD) camera is mounted on the 2Θ circle of a compact diffractometer carrying the sample on its ω circle. The asymmetric cut of the analyzer crystals was chosen in order to provide 40-fold magnification at Cu $K\alpha_1$ radiation ($\lambda = 1.5406$ Å), which allowed testing the apparatus in the laboratory. The same wavelength was then used for the synchrotron experiments at the topography beamline ID19 of the European Synchrotron Radiation Facility (ESRF).

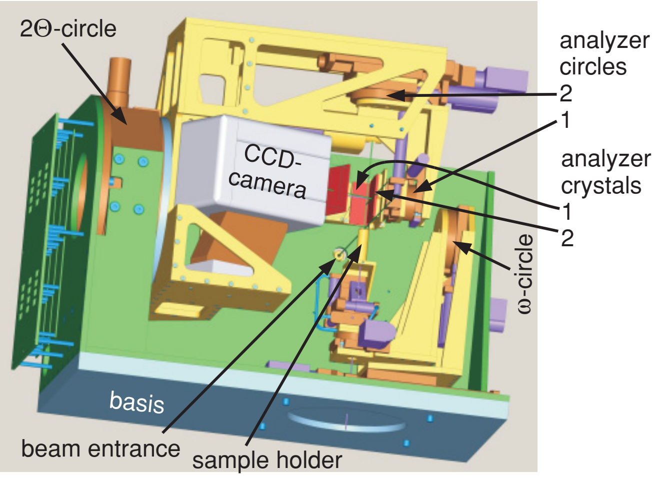

FIG. 3. (Color online) Sketch of the topomicroscope.

As shown in Fig. 3 the entire TM is mounted on a base plate, which can be easily fixed to a work table at the beamline. The x-ray beam enters the TM parallel to the base plate and the side edge of the box. The sample is mounted on the holder fixed on an ω circle. Additional degrees of freedom are the azimuthal rotation and x-z movement. The 2Θ circle carrying the TM is only used for the initial 2Θ adjustment because of limited accuracy due to the weight of the TM setup. 2Θ rocking curves are taken by rotating the first analyzer. The second analyzer offers a rotation in the diffraction plane, which corresponds to a θ_2 scan, and can also be shifted in one direction and rotated in order to precisely achieve perpendicular diffraction planes of the first and second analyzers.

The field of view for the topomicroscope was about 1 mm^2 and was set in the range of the central triple line in Fig. 2. The cuts used in the following are chosen so as to show the complete length of one seed window.

For all measurements with the TM a symmetric (333) reflection was used at the sample. At an x-ray wavelength equivalent to Cu $K\alpha_1$ radiation, a 40-fold magnification at both analyzers of the TM is obtained. Since the TM probes under an exit glancing angle of 47.47°, the y direction (i.e., within the sample diffraction plane) appears reduced by a factor of 0.737. All pictures are corrected correspondingly.

For the following it is essential to refer to a problem with the evaluation of the TM experiments. Previously we have demonstrated a strong dispersive interaction of both analyzer crystals in the Bragg magnifier.[12] Actually, the angular position on the rocking curve of one analyzer crystal determines the wavelength bandwidth that is available to the other one. This effect results in the fact that the full width at half maximum of one rocking curve depends on the angular offset of the other. Similarly, the observable peak position of one rocking curve depends on the angular position of the other. It seems intuitively clear that the situation becomes even more complex when a third crystal (the sample) is introduced. A local rotation of its net planes (due to deformation within the diffraction plane) yields a rocking curve shift at the sample itself as well as on the first analyzer crystal. However, local sample rotations about an axis parallel to the the seed window have only a second-order influence on the Bragg condition at the sample or at the first analyzer. Such a local tilt in the sample relative to the sample diffraction plane is measured by a Θ_2 scan with the second analyzer (diffraction plane perpendicular to that of the sample). In order to avoid the problems related to the above-mentioned dispersive interaction we will demonstrate in the next section that in the given case measurements by means of the second analyzer are nearly undisturbed by this interaction and therefore are well suited for data evaluation.

IV. RESULTS

In the following we will focus on the smaller lamella (referring to a 500 μm seed window) as shown in the upper (or lower) region of Fig. 2. The cuts used in the following are chosen to show the complete length of one seed window. Figure 4 shows a topograph taken with the TM. Due to its superior spatial resolution and the high collimation of the synchrotron radiation in both directions, there are far more details visible than in the conventional topograph of Fig. 2. The seed windows are clearly depicted and there are distinct deformation-related contrasts near to and on the edges of the lamella. Roughly perpendicular to the seed window a wavy contrast (w) appears, indicating that there is a corresponding modulation of the forces drawing the lamella toward the substrate. Additionally a stripe pattern (s) can be observed, which runs about parallel to the upper lamella edges in Fig. 4. The geometrical arrangement seems to indicate that these stripes follow the growth front at some time intervals. This could mean that the lateral growth velocity was not constant, but somewhat modulated.

Figure 5 gives the local rocking curve shift from an ω scan (while scanning the sample) with the seed windows parallel to the sample diffraction plane. Without taking the explained effect into account, we should expect a picture that appears to be mirror-symmetric with respect to the seed window.

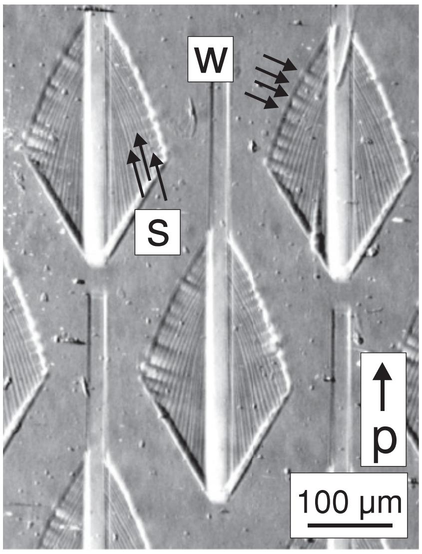

FIG. 4. A topograph taken with the TM at the low-angle flank of the sample rocking curve. Arrow (p) gives the projected incidence direction of the synchrotron beam on application of the (333) reflection at $\lambda = 1.5406$ Å. Hence the diffraction planes are parallel to the seed windows.

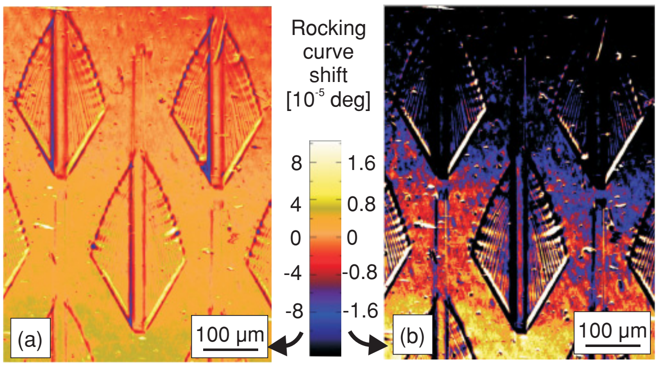

FIG. 5. (Color online) Bragg angle differences at a sample ω scan evaluated by means of the centers of gravity of the local rocking curves. (a) Full and (b) reduced scale.

However, judging from the general trend of the three visible lamella in Fig. 5, it becomes rather obvious that there are distinct deviations from this naive expectation.

Figure 5(a) clearly shows a stronger elastic deformation near the seed window and the lamella edges compared to any other position. Due to the superior resolution details of this prominent effect can be further resolved with respect to previous measurements.[14] The corresponding deformations are about an order of magnitude lower than those visible in Fig. 5(a). Weaker effects become visible only if the scale of the rocking curve shifts is reduced as in Fig. 5(b). The changes in the background, i.e., the signal from the undisturbed substrate, are due to the mean curvature of the sample and to a Bragg angle shift caused by dispersion.

The rather pure case mentioned at the end of Sec. III is shown in Fig. 6, a Θ_2 scan with the second analyzer. Its diffraction plane is perpendicular to the seed window. As each single ELO structure is mirror symmetric with respect to the seed window, a local rotation around an axis *parallel* to the seed window should produce *antisymmetric* effects. On the other hand, local lattice parameter differences or rotations around an axis *perpendicular* to the window may produce *symmetric* effects. Both are, of course, related to the seed window itself.

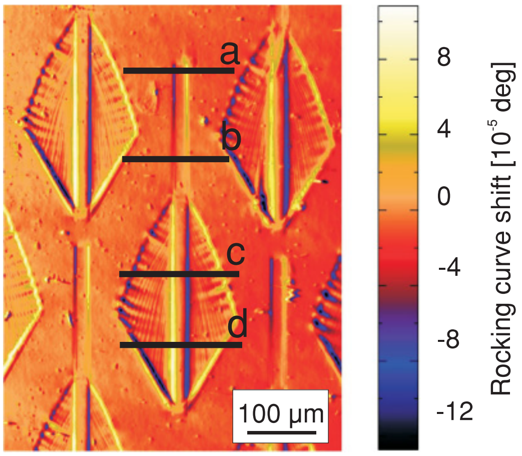

FIG. 6. (Color online) Rocking curve shifts at a Θ_2 scan extracted by the centers of gravity of the rocking curves. Lines *a* to *d* refer to the rocking curve scans in Fig. 8.

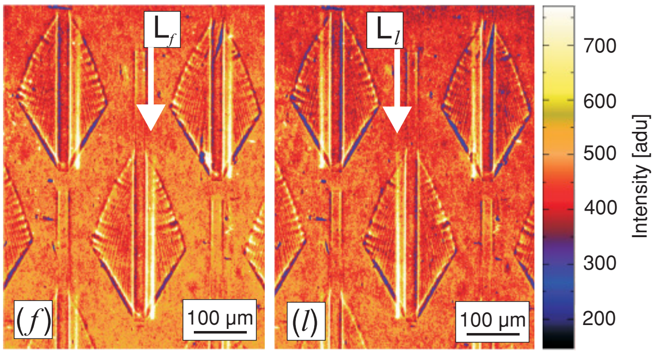

FIG. 7. (Color online) First (*f*) and last (*l*) topographs of a Θ_2 scan, corresponding to $\mp 0.01^\circ$ relative to the Bragg peak. The intensity is given in analog-to-digital units (adu). About 4 adu correspond to a single x-ray photon of the given wavelength.

Actually, the effects are predominantly antisymmetric; thus they are mainly due to a local lattice rotation around an axis parallel to the seed window. Now the question arose as to whether these effects are basically related to the substrate itself or to the strongly curved epitaxial layer.[14] Figure 7 compares the first (*f*) with the last (*l*) topograph of the scan that led to Fig. 6. At angles smaller than the Bragg angle Θ_B, the lamella reflection appears as a narrow stripe (L_l) on the right of the seed window, but at angles larger than Θ_B on the left, marked (L_f). Therefore nearly everywhere on the ELO structure the substrate and the lamella reflections are well separated and the peak of the latter is much lower due to the strong curvature. This means that mainly the substrate reflection is probed.

As mentioned in Sec. I the most interesting positions are the lateral layer edges and the seed window edges. In the following we will focus on the seed window edges for the following reasons: First the deformation contrast is stronger than on the layer edges and second there is a contrast at the oxide edges in the regions where there is practically no epitaxial layer present, e.g., at the upper end of the central seed window in Fig. 6. The latter can be used for a comparison with the known forces at the oxide edges. However, we have to admit that there is some tradeoff: this is just the position where it becomes difficult to separate contrasts due to deformation in the layer and the substrate. Figure 8 depicts rocking curves along the scan lines *a*–*d* in Fig. 6. In Figs. 8(c) and 8(d) weakly inclined streaks are present in the region close to the seed window. These are due to the lamella reflections. Due to the nearly uniform curvature of the lamella in this range the streaks on the left and the right sides are lying approximately on a straight line. Its lower and upper crossing with the diagram frame refers to the position of the lamella reflection in Fig. 7. Therefore, we can state that besides this superimposed course of the lamella reflection the shift of the rocking curve is solely due to the substrate reflection.

Figure 8 nicely shows the mainly antisymmetric deformation at the seed window edges (and also on the lamella edges). This is especially interesting since this deformation changes its sign if Fig. 8(a) is compared with Figs. 8(c) and 8(d). In the range of Fig. 8(a) there is practically no epitaxial layer within the seed window and the deformation of the substrate is due to the compressive stress in the oxide layer. Rather

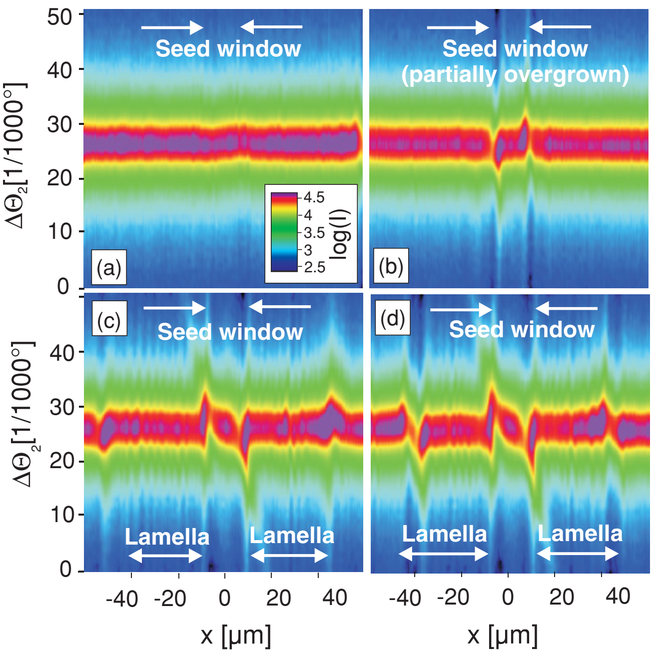

FIG. 8. (Color online) Rocking curves along the x axis in Fig. 6 lines a to d. The scale gives the angular position in relation to the angular position of the first topograph of the scan. Please note the tilted streaks close to the seed window edges, which are due to the lamella reflections.

different values for this stress are given in the literature.[18,19] However, as a standard oxidizing procedure was used, the stress is here probably about −0.3 GPa. The deformation in Figs. 8(c) and 8(d) has a quite similar signature, but with opposite sign and twice the value, which clearly indicates tensile stress.

For the following discussion the transmission electron micrograph in Fig. 9 will provide additional information. It shows a series of inclusions at the interface between substrate and epitaxial layer. By means of strain investigation these were identified as SiO_x. This micrograph clearly reveals that residual oxygen concentrates at a few inclusions at the substrate-lamella interface.

V. DISCUSSION

A first hypothesis to explain the curvature of the epitaxial layer in the Si/SiO_x/Si system refers to adhesion, which exerts forces at the growth front.[6] The comparatively strong deformation at the lamella edges, demonstrated in Fig. 6, fits quite well into this description. On the other hand, the deformation at the edges of the seed window is even stronger. This is not necessarily a contradiction, but arouses some suspicion about the strength of the effect. For the system GaAs/SiO_x/GaAs the curvature of the epitaxial layer becomes weaker by a factor of 100 if SiO_x is replaced by graphite.[20] This might be due to the fact that the solvent does not wet the graphite.[21] A further alternative could be that graphite more effectively relaxes elastic stress. But there is even a third option: graphite is a rather stable material without any tendency to diffuse into the surroundings, which is one of the reasons to use graphite as the container material for LPE. On the other hand, it is well known that oxygen within SiO_x can diffuse, as was discussed for the residual oxygen at the interface in the case of wafer bonding.[22] Similarly, Fig. 9 demonstrates that residual oxygen at the substrate–epitaxial-layer diffuses and forms precipitates.

Therefore, oxygen diffusion from the SiO_x layer might be a key reason for the observed strain state. In the case of LPE Si/SiO_x/Si there are two possible drains: the solvent and the epitaxial layer itself. The hydrogen-containing atmosphere in the growth container may play a role in the process as well. Considering LPE Si/SiO_x/Si as a model system for the explanation of curvature and tilt of the epitaxial layer in GaN ELO, the vacuum might be the drain for oxygen diffusion. Furthermore, one can argue that the surface of the epitaxial layer will have some catalytic influence.

While the deformation at the seed window in Fig. 8 appears highly antisymmetric, there is a significant symmetric contribution at the lamella edges at line d in Fig. 6. This means that here a considerable vertical stress should be present, resulting in a corresponding lattice parameter change in the substrate.

Therefore we decided to use a model where we have applied different strain states to the oxide layer. The corresponding elastic deformation field is calculated by means of the finite-element method (FEM).

The general FEM model as depicted in Figs. 10(a) and 10(b) is based on a regular 100 nm grid (not shown in Fig. 10). Please note that x-ray diffraction does not prove to be very sensitive to the near field of the deformation, but to the far field on a length scale of micrometers instead. We have checked that scaling works reliably due to this effect. With the model of Fig. 10(a) we changed the strain state of the oxide layer by one grid step thickness at a time until the contrast simulations (see the Appendix) based upon the FEM models fit well with the measurement scans around the seed window (see the comparison in Fig. 11). For comparison, we have also investigated the case without an epitaxial layer. Good agreement was achieved with an expansion of the oxide relative to the substrate of 2×10^{-3} in the sample. This corresponds to an elastic stress of approximately 0.3 GPa, taking the Young's modulus (68 GPa), a Poisson ratio of 0.202, and a scaling factor of 1.54 (the true oxide thickness is 65 nm) into account. This corresponds well with the value of 0.3 GPa given in Ref. 19.

The nearly complete contrast extinction at the oxide edges at line b in Fig. 6 was puzzling. Here the models were calculated

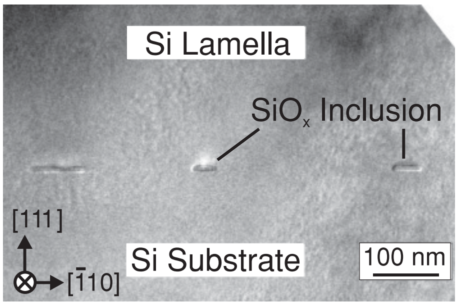

FIG. 9. Transmission electron micrograph of SiO_x inclusions at the substrate-lamella interface.

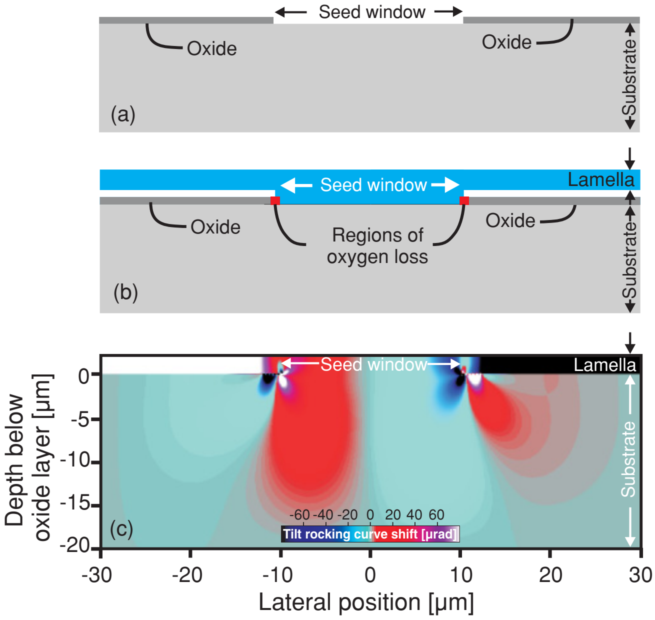

FIG. 10. (Color online) Models used for finite-element calculations: (a) Without any epitaxial layer, corresponding to the situation in scan *a* of Fig. 6 or Fig. 8(a), respectively. (b) With epitaxial layer: there is an empty layer below the lateral overgrowth, where vertical forces are applied in order to achieve the same lamella curvature as observed in the experiment. One grid square (red colored) is used to simulate an oxide layer with oxygen loss. (c) The local tilt assuming model (b). All tilts larger than 100 μrad have been cut for better view. Please note that the angular difference between overgrowth lamella and substrate increases to values beyond 100 μrad about 3 μm to the left from the oxide layer edge.

with an epitaxial layer of 1 μm thickness restricted to the seed window. All models with some strain relaxation in the oxide layer close to the edge failed completely. However, as shown in Figs. 11(c) and 11(d), there is good agreement if an expansion of the epitaxial layer of 4×10^{-5} is assumed. The most probable impurity in the epitaxial layer is indium. Apparently, there are no studies on the silicon lattice constants in dependence on indium content. The covalent radii $r_{\mathrm{Si}} = 0.1173$ nm and $r_{\mathrm{In}} = 0.1405$ nm (Ref. 23) yield $n_{\mathrm{In}} = 2.53 \times 10^{23}(da/a)_{\mathrm{relax}}$, i.e. in the given case $n_{\mathrm{In}} = 4 \times 10^{18}$ atoms/cm^3. However, the investigated sample has a nominal boron content of 2×10^{18} atoms/cm^3. In Ref. 24 the lattice contraction of boron-doped epitaxial silicon was determined by x-ray diffraction, and a contraction value of $\beta = 5 \times 10^{-24}$ cm^3/atom was found, in agreement with most values given in the literature before. The nominal boron content results then in (strain $\epsilon = \beta c_{\mathrm{In}}$ as used in Ref. 24) $(da/a) = -1 \times 10^{-5}$. Taking this into account the resulting indium content is reduced to 1.5×10^{18} atoms/cm^3. This seems to be a rather high value. This lattice expansion was then another parameter to be taken into account for further FEM calculations.

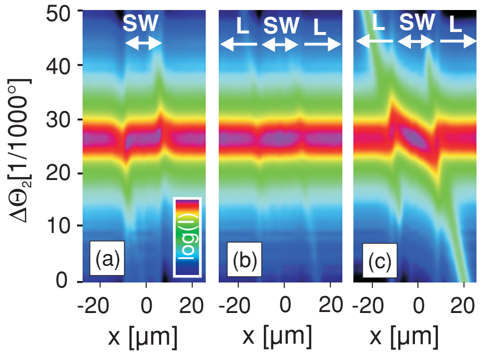

FIG. 11. (Color online) Rocking curve simulations based on FEM calculations. (a)–(c) are to be compared with Figs. 8(a)–8(c). For the simulation procedure see the Appendix and for the values used for the FEM see text.

Of course, most interesting is the case corresponding to line *c* or *d* in Fig. 6. We have focused on the first one. Here the thickness of the epitaxial layer is 2 μm. However, as discussed in the Introduction by means of the zipper analogy, this case cannot give directly the forces bending down the overgrowing epitaxial layer but only the situation after overgrowth. Therefore, above the oxide layer an empty layer of one grid step height was placed to allow for bending of the lamella as observed in the experiment. The forces keeping the overgrowth layer in its bent state are approximated by opposite face loads acting on the lower face of the epitaxial layer and the upper face of the oxide. Again, an attempt to explain the contrasts solely by some oxide relaxation or stress state inversion close to the oxide edge failed. Good agreement [see Fig. 11(c)] was eventually achieved with the following parameters: Inversion of the strain state of the oxide layer relative to the substrate of -2×10^{-3}, linear increase of tensile strain toward the oxide edge of -8×10^{-3} over a distance of 2 μm, a face load of 5×10^{-5} GPa as a tensile stress between epilayer and oxide in the outer half of the model overgrowth layer and the same expansion stress in the inner half, and an expansion of the epitaxial silicon of 2×10^{-5}.

The upward-directed peak at the left oxide edge in Fig. 11(c) indicates a tensile stress at the oxide edge, the much smaller one directed downward to a compressive stress. The mentioned linear increase used in the calculation produces this small peak, because it introduces a weak dipole force. The actual profile of this increase is certainly not very reliable; however, the general tensile stress in the oxide layer cannot be changed without changing the contrast in the simulation significantly. The value of this tensile stress seems to vary on a scale of some micrometers, as the oscillations in the measurement scan show. However, the general tensile component is preserved to the outer edge of the epitaxial layer. Comparing the contrast at the left outer edge of the epitaxial layer in scan *c* of Fig. 6 with the contrast at the left oxide edge in scan *a* in Fig. 6 lets us estimate the stress at approximately the same value, i.e., the tensile stress persists under the overgrowth lamella. With the elastic parameters given before, the corresponding tensile stress is approximately 0.3 GPa, increasing toward about 1.2 GPa at the oxide edge.

There is a significant difference in the contrasts at the outer edge of the overgrowth lamella in Fig. 6, lines *c* and *d*, and Figs. 8(c) and 8(d), respectively. This is related to the fact that lateral overgrowth starts first at the highest area of the epitaxial layer within the seed window, as already discussed in Ref. 9. The shape of the lamella develops as indicated by the narrow lines (s) in Fig. 4. That is, the $\{111\}$ facets in the area around line *d* are present from the start of overgrowth on, whereas these facets in the area around line *c* are formed with completion of the overgrowth. The symmetric contribution to the contrast at the outer edge of the lamella at line *d* indicated the presence of significantly stronger vertical forces as compared to the case of line *c*.

In a rough approximation the oxygen loss can be estimated by assuming that at about equal volume contributions of silicon and oxygen in the oxide the volume shrinks about half as fast as the oxygen content. With the above-mentioned values and thickness correction, the relative volume change amounts to 0.6% in the oxide layer and to about 2.2% at the oxide edge. Consequently the relative oxygen loss of the oxide should amount to about 1.2% and 4.4%, respectively.

In this context we have to stress that according to our results a general oxygen depletion of the oxide layer cannot explain why the compressive strain at the oxide edge at line *a* of Fig. 6 is preserved, whereas it is converted to tensile stress at the oxide edge as well as on the edge of the overgrowth layer at line *c*. In our opinion the only explanation is that this conversion happens at the growth front during lateral overgrowth. An oxygen loss directly at the growth front, i.e., below the outermost part of the overgrowing lamella, will lead to a slight vertical shrinking of the oxide layer. This will then quite naturally result in bending the overgrowing lamella toward the substrate.

As our results are deduced from the evaluation of deformations we cannot exclude the possibility that adhesion forces at the growth front are responsible for the results. However, the fact that the forces acting on the substrate are mainly directed along the surface speaks against this explanation and favors the explanation by oxygen loss.

It seems reasonable that a similar oxygen depletion happens in the case of GaN ELO over a silicon oxide layer. The stresses related to the contrasts in Fig. 6 and the corresponding contrast simulations in Fig. 11 explain then quite naturally why threading dislocations concentrate at the seed window edges in the case of GaN ELO.

VI. SUMMARY

From the results we can exclude a general shrinkage of the oxide as proposed in Refs. 7,8 because this would not explain the persisting compressive strain at the oxide edge in position *a* of Fig. 6 or in Fig. 8(a). On the other hand a mutual relation between oxygen loss and the growth process appears rather reasonable. Such a dependence can nicely explain the general curvature of the lateral epitaxial overgrowth. Further, FEM calculations yield a loss of about 1% in the oxide layer, increasing to about 4% toward the oxide edge at the seed window. The FEM calculation also numerically delivers a tensile stress at the edge on the order of 1 GPa. This seems to be too large to explain the curvature exclusively by means of adhesive forces as previously proposed.[5,6] The experimentally observed and numerically described tensile stress at the oxide edge convincingly explains why dislocations concentrate at the oxide edges and lead to a tilt of the lateral epitaxial layer during the ELO of GaN.

ACKNOWLEDGMENTS

We are indebted to Gerd Schadow, Institute for Crystal Growth, Berlin for his technical support. The authors acknowledge financial support by the German Research Foundation (DFG), Grants No. KO1510/6-1, No. BO1129/4-1, and No. HA3495/3-1. We thank the European Synchrotron Radiation Facility (ESRF) in Grenoble, France for providing beam time (MA-292). Finally, we would like to thank Alexander Rack (now at the ESRF) for assistance during manufacturing of the topomicroscope.

APPENDIX

A comprehensive treatment of the contrast formation would require a three-dimensional Takagi-Taupin calculation taking into account wave propagation from sample to second analyzer. However, the rather obvious antisymmetry of the measurements (compared to the real-space shape symmetry) shows that tilt effects outweigh by far diffraction effects in the diffraction plane of the sample. These should, on the other hand, yield symmetric effects in Fig. 8. Therefore, it seems reasonable to try a simple approximation: adding up the contributions of points in the depth of the sample and taking into account the exponential intensity decrease with depth in the Bragg case. Looking backward from a point on the second analyzer crystal (responsible for measurement of the local sample tilt), the first Fresnel zone on the sample at about 95 mm distance has a width of only 1.4 μm. Furthermore there is a finite angular acceptance width of the sample. Both effects seem to indicate that summation of the intensities might be adequate, and both effects are taken into account in the calculation within a ray tracing approximation. Each position in the FEM data set is attributed to a rocking curve of the second analyzer as measured in the unstructured region of the sample. Its intensity is reduced exponentially using 10 μm penetration depth. A local tilt in the FEM data is taken into account by a rocking curve shift. Use of a 5 μm penetration depth does not change the results noticeably. Obviously, the results as shown before confirm that this approximation is a reasonable one. We have also considered summing the amplitudes; however, without taking into account phase differences according to the just mentioned effects. This gives only minor differences from the intensity summation.

At the symmetric reflection with a Bragg angle of 47.47° at the sample, any tilt in the sample results in a tilt of the reflected beam larger by a factor of 1.47. This is taken into account in the comparisons shown above, i.e., there the resulting values in the sample are given.

---

[1] M. Seon, T. Prokofyeva, M. Holtz, S. A. Nikishin, N. N. Faleev, and H. Temkin, Appl. Phys. Lett. **76**, 1842 (2000).

[2] S. Nakamura, M. Senoh, N. Iwasa, S. Nagahama, T. Yamada, and T. Mukai, Jpn. J. Appl. Phys. **34**, L1332 (1995).

[3] F. Wang, R. Zhang, W. S. Tan, X. Q. Xiu, D. Q. Lu, S. L. Gu, B. Shen, Y. Shi, X. S. Wu, Y. D. Zheng, S. S. Jiang and T. F. Kuech, Appl. Phys. Lett. **80**, 4765 (2002).

[4] O. Nam, M. D. Bremser, T. S. Zheleva, and R. F. Davis, Appl. Phys. Lett. **71**, 2638 (1997).

[5] H. Raidt, R. Köhler, F. Banhart, B. Jenichen, A. Gutjahr, M. Konuma, I. Silier, and E. Bauser, J. Appl. Phys. **80**, 4101 (1996).
[6] R. Köhler, B. Jenichen, H. Raidt, E. Bauser, and N. Nagel, J. Phys. D **28**, A50 (1995).
[7] H. Marchand, X. H. Wu, J. P. Ibbetson, P. T. Fini, P. Kozodoy, S. Keller, J. S. Speck, S. P. DenBaars, and U. K. Mishra, Appl. Phys. Lett. **73**, 747 (1998).
[8] P. Fini, H. Marchand, J. P. Ibbetson, S. P. DenBaars, U. K. Mishra, and J. S. Speck, J. Cryst. Growth **209**, 581 (2000).
[9] R. Bergmann, J. Cryst. Growth **110**, 823 (1991).
[10] A. Sakai, H. Sunakawa, and A. Usui, Appl. Phys. Lett. **73**, 481 (1998).
[11] D. Lübbert and T. Baumbach, J. Appl. Crystallogr. **40**, 595 (2007).
[12] P. Modregger, D. Lübbert, P. Schäfer, J. Richter, R. Köhler, and T. Baumbach, Opt. Express **17**, 11618 (2009).
[13] R. Bergmann, E. Bauser, and J. H. Werner, Appl. Phys. Lett. **57**, 351 (1990).
[14] B. Heimbrodt, D. Lübbert, R. Köhler, T. Boeck, A. Gerlitzke, and M. Hanke, Cryst. Res. Technol. **44**, 534 (2009).
[15] D. Lübbert, T. Baumbach, J. Härtwig, E. Boller, and E. Pernot, Nucl. Instrum. Methods **160**, 521 (2000).
[16] D. Lübbert, T. B. P. Mikulik, P. Pernot, L. Helfen, R. Köhler, T. M. Katona, S. Keller, and S. P. DenBaars, J. Phys. D **38**, A50 (2005).
[17] P. Modregger, D. Lübbert, P. Schäfer, and R. Köhler, Phys. Rev. B **74**, 054107 (2006).
[18] I. A. Blech and E. Meieran, J. Appl. Phys. **38**, 2913 (1967).
[19] A. Szekeres and P. Danesh, Semicond. Sci. Technol. **11**, 1225 (1996).
[20] Z. R. Zytkiewicz, J. Domagala, D. Dobosz, and J. Bak-Misiuk, J. Appl. Phys. **84**, 6937 (1998).
[21] Z. R. Zytkiewicz, J. Domagala, and D. Dobosz, J. Appl. Phys. **90**, 6140 (2001).
[22] K. Y. Ahn and U. Gösele, J. Electr. Eng. **17**, S19 (1988).
[23] J. A. van Vechten and J. C. Phillips, Phys. Rev. B **2**, 2160 (1970).
[24] H.-J. Herzog, J. Electrochem. Soc. **131**, 2696 (1984).